Accuracy Analysis of Photogrammetric UAV Image Blocks: Influence of Onboard RTK-GNSS and Cross Flight Patterns

MARKUS GERKE, Enschede, The Netherlands & HEINZ-JÜRGEN PRZYBILLA, Bochum

Summary: Unmanned aerial vehicles (UAV) are increasingly used for topographic mapping. Despite the flexibility gained when using those devices, one has to invest more effort for ground control measurements compared to conventional photogrammetric airborne data acquisition, because positioning devices on UAVs are generally less accurate. Additionally, the limited quality of employed end-user cameras asks for self-calibration, which might cause some problems as well. A good distribution of ground control points (GCPs) is not only needed to solve for the absolute orientation of the image block in the desired coordinate frame, but also to mitigate block deformation effects which are resulting mainly from remaining systematic errors in the camera calibration. In this paper recent developments in the UAV-hardware market are picked up: some providers equip fixed-wing UAVs with RTK-GNSS-enabled 2-frequency receivers and set up a processing pipeline which allows them to promise an absolute block orientation in a similar accuracy range as through traditional indirect sensor orientation. Besides the analysis of the actually obtainable accuracy, when one of those systems is used, we examine the effect different flight directions and altitudes (cross flight) have onto the bundle adjustment. To this end two test areas have been prepared and flown with a fixed-wing UAV. Results are promising: not only the absolute image orientation gets significantly enhanced when the RTK-option is used, also block deformation is reduced. However, remaining offsets originating from time synchronization or camera event triggering should be considered during flight planning. In flat terrains a cross flight pattern helps to enhance results because of better and more reliable self-calibration.

Zusammenfassung: *Genauigkeitsuntersuchung von photogrammetrischen UAV-Bildverbänden: Einfluss von onboard RTK-GNSS und Kreuzflugmustern.* Flugroboter (unmanned aerial vehicles, UAV) werden zunehmend zur topographische Kartierung eingesetzt. Die Systeme weisen eine hohe Flexibilität auf, jedoch muss im Gegensatz zu konventionellen Befliegungen mehr Aufwand in die Erfassung von Kontrollpunkten am Boden investiert werden. Der Grund dafür liegt in der schlechteren Qualität der Positionierungslösungen auf dem Flugroboter. Hinzu kommt, dass die verwendeten Kameras eine unbekannte geometrische Stabilität haben, und die Parameter der Inneren Orientierung normalerweise nicht hinreichend genau fixiert sind. Die Folge ist, dass eine Selbstkalibrierung im Rahmen der Bündelausgleichung durchgeführt werden muss. Diese Selbstkalibrierung ist nicht in jedem Anwendungsfall zuverlässig. Eine gute Verteilung von Kontrollpunkten ist nicht nur für die Bestimmung der Lagerung des Bildverbandes notwendig sondern auch um Blockdeformationen zu verringern. Diese entstehen größtenteils durch bei der Kamerakalibrierung verbliebene systematische Fehler. In diesem Beitrag greifen wir aktuelle Entwicklungen im UAV-Markt auf: einige Hersteller rüsten ihre Geräte mit einem RTK-fähigen 2-Frequenz-GNSS-Empfänger aus und bieten einen entsprechenden Prozessierungsablauf

an. Sie versprechen dadurch Genauigkeiten in einem Bereich ähnlich der traditionellen indirekten Sensorpositionierung zu erhalten. Neben der Analyse der tatsächlich erreichbaren Genauigkeit eines dieser Systeme untersuchen wir den Effekt, den verschiedene Flugrichtungen und –höhen auf die Blockausgleichung haben (Kreuzbefliegung). Zu diesem Zweck wurden zwei Testareale vorbereitet und mit einem unbemannten Flächenflugzeug beflogen. Die Ergebnisse sind vielversprechend: durch die Nutzung der RTK-Option wird nicht nur die absolute Blockorientierung signifikant verbessert, auch werden die Blockdeformationen reduziert. Es sollten jedoch verbleibende Fehler, die durch ungenaue Synchronisation der Sensorbeobachtungen oder Kameraauslösung entstehen, bei der Flugplanung berücksichtigt werden. In flachen Gebieten hilft die Kreuzbefliegung die Ergebnisse zu verbessern, da eine bessere und zuverlässigere Selbstkalibrierung durchgeführt werden kann.

1 Introduction

The derivation of topographic information from unmanned aerial vehicles (UAV) is becoming increasingly interesting for routine tasks in the geomatics domain. Digital surface models (DSM) or ortho images are standard products. Especially for the acquisition of relatively large image blocks (some 100+ hectares) small fixed-wing UAVs are used (COLOMINA & MOLINA 2014). In this paper we use the term UAV, but in literature we find also terms like UAS (unmanned aerial system) or RPAS (remotely piloted aerial system). In the scope of this article all those abbreviations are treated as synonyms. More specifically we refer to small UAV which are devices with an overall weight of up to 25 kg (NEX & REMONDINO 2014, WATTS et al. 2012). Small UAVs being easily deployed require only small training efforts and in many countries regulations are in place which allow for a convenient permission issuance.

The main advantages of small UAVs over traditional (manned) airborne-based mapping are: i) flexibility – individual flight patterns can be realized; ii) unrivalled image resolution – a ground pixel size of 5 cm, mostly smaller, can easily be achieved; iii) ease of use – with a small training effort, state-of-the-art devices can be operated even by laymen. However, compared to established workflows based on manned airborne photography, some issues need to be considered. Because of weight and cost restrictions, sensor devices used in UAVs (positioning, camera) are normally of much lower quality compared to professional sensors employed in manned airborne systems. This has as the consequence that in order to achieve the best accuracy for the final mapping product, a significant amount of work concerning signalization and measurement of ground control points (GCPs) is needed. In this context some recent developments concerning GNSS localization are interesting: there is the tendency towards RTK (Real Time Kinematic) devices being integrated onboard commercially available UAV. This means that in fact, survey-grade direct sensor positioning of UAV images is available for the mass market. Opposed to DGPS, which only considers code-based observations in addition to differential corrections, the RTK approach incorporates phase measurements which promise absolute accuracy in the sub-cm range.

Another issue to be addressed when capturing UAV-based image blocks is the necessity to estimate intrinsic camera parameters during bundle adjustment (self-calibration). This process adds another source of uncertainty, because the physical stability of the camera as such is unknown. Moreover, if the area of interest is largely flat, the estimate of the principal distance might be very inaccurate due to the high correlation of the Z-component and focal length in nadir viewing geometry. From literature we know that so-called cross flight patterns and different flying heights might render the self-calibration process more reliable (CRAMER 2001).

In this paper we present results from experiments which were conducted in several setups in order to address the practically relevant questions concerning a) the influence of cross flight patterns on the overall bundle block adjustment quality and b) the role of GCP distribution on the ground, especially in conjunction with using a RTK-GNSS-enabled commercial fixed-wing UAV. In addition, we analyse the impact those different configurations have on the camera self-calibration.

In an earlier work by PRZYBILLA et al. (2015) already some of the points were addressed. In the paper at hand the experiments are explained in more detail and extended towards a more quantitative evaluation of the RTK-based localization solution and different flight configurations. To this end, several test scenarios, applied in different terrain, are defined and analysed.

In the next section some related research on UAV image block orientation, both using indirect methods, but also referring to onboard positioning solutions, is described. Section 3 elaborates on the data processing workflow as implemented by the system used in our experiments. The subsequent section describes the datasets used, while section 5 focusses on the results. The last section provides some discussion and conclusions.

2 Related Work

In many related papers the usage of GCPs to support indirect sensor orientation of UAV-based image blocks is analysed. One consideration refers to the positional accuracy which is needed at GCPs.

If pixel-level absolute accuracy is aimed for in image orientation, it implies a need for appropriate reference information. Nowadays, a GSD of 2 cm – 3 cm is easily achievable in UAV projects, meaning that 3D points on the ground need to be measured with at least state-of-the-art GNSS-RTK technology or engineering survey-ing methods based on total stations. In addition there is a need to differentiate between approaches which only apply a 3D-similarity transform to the entire UAV-image block and those which employ control information within the bundle block adjustment, e.g. as soft constraints. The former one is in principle easier to realize but keeps the risk that block deformations within the initial UAV-solution do not get adjusted (NEX & REMONDINO 2014). In other papers, large errors are reported especially in the Z-component when only a 3D-similary trans-form is performed (NOCERINO et al. 2013, RUMPLER et al. 2014). When GCPs were introduced into the bundle adjustment the errors were reduced by a factor of 3, and they became even smaller when oblique images were used. Those oblique images provide an image block geometry which also supports self-calibration (NOCERINO et al. 2013).

However, to reduce the workload when dealing with UAV campaigns the desire to obtain reliable results, but without large effort on ground control measurements, is obvious. In literature we find many different approach-es to obtain reliable and accurate image orientation parameters within the given mapping frame, but without the use of GCPs and advanced onboard positioning hardware. FÖRSTNER & STEFFEN (2007) used an existing DSM to fine-register an UAV-block based on the UAV-derived DSM. Although they achieved overall good quality in their experiment, the block deformation issue remains unsolved and the requirements on the terrain as such are quite demanding, because the terrain structure should show height gradients in different directions and of dif-ferent strength to allow for an unambiguous and adequate co-registration. More recently, YANG & CHEN (2015) co-registered a point cloud derived from UAV-based image sequences to LiDAR data over urban areas. Build-ing outlines are detected in the images as well in order to colourize the LiDAR-based point cloud. The image orientation was performed with an average error of about 0.5 pixels, as reported for different test sites. This is a reasonable result, but still there is a need for existing LiDAR data and demands on the topography are similar to the ones listed in FÖRSTNER & STEFFEN (2007). This observation leaves us with the conclusion that, in order to have a generally applicable workflow for indirect orientation of UAV image blocks, still individual, highly accurate GCPs are needed, possibly in combination with a flight configuration which supports accurate self-calibration.

Other works analysed methods on how onboard GNSS and IMU can be integrated in the UAV workflow, in order to derive a better direct estimation of the position and attitude of the aircraft. PFEIFER et al. (2012) per-formed some preliminary tests using a low-cost onboard IMU and GNSS receiver and achieved a platform position accuracy better than 1 m. ELING et al. (2014) describe a prototype where RTK-GNSS, a second GNSS receiver for heading estimation, and a low cost IMU (MEMS-based) are integrated into a real-time position estimation approach. In the experiments the authors achieved a standard deviation of 1 cm to 2 cm in position and up to 1.5° in absolute angle measurements. REHAK et al. (2014) report about a similar system and obtained similar accuracy values, but the system was not capable of delivering results in real-time. A different approach to direct sensor orientation is to use visual odometry, i.e. to employ stereo cameras for accurate (relative) atti-tude and position estimation. SCHNEIDER et al. (2014) combine such a method with RTK-GNSS to solve for the unknown position, rotation and scale within the mapping frame.

While the mentioned literature describes successful research prototypes, we can also observe that today UAV-vendors offer complete systems which integrate survey-grade RTK-GNSS localization on board the UAV. For instance, the Topcon B110 board is used in the Mavinci Sirius Pro, and the Sensefly Ebee RTK (MAVINCI 2015, SENSEFLY SA 2015). Research showed that with this RTK-GNSS board it is possible in principle to assign to each camera exposure a position estimation in the range of 2 cm – 3 cm accuracy, i.e. much better than a standard DGPS solution (BÄUMKER et al. 2013). By now many more UAV-system vendors offer RTK-GNSS-enabled systems. However, in 2014, when the experiments for this paper were conducted, only the Mavinci system was available.

Within the bundle adjustment the RTK-GNSS observations assigned to each image would not only help to solve for the exterior image orientation in the given mapping frame, but also mitigate block deformation effects.

Although the aforementioned research papers proved the positive influence of those direct observations onto the bundle block adjustment, a systematic analysis of commercially available systems has still not been carried out to our knowledge. The use of commercial systems has the advantage that experiments can be reproduced and have a larger relevance for practical applications.

3 Details on the RTK-supported Workflow

Many factors influence the accuracy of the position which is assigned to an image taken during the UAV flight. As the GNSS-RTK board can deliver an absolute position at 2 cm – 3 cm error level, the goal must be to minimize the remaining error coming from uncertainties of the relative alignment of the sensors on board of the UAV and data processing. The following components play an important role in this respect: calibration of offset from camera projection centre to antenna phase centre (boresight alignment), attitude of plane during exposure time, time synchronization, and last but not least a method to identify blunders during bundle adjustment.

As our dataset is from the Mavinci Sirius Pro system, we give details about the workflow implemented by this provider. The calibration of offsets from the camera projection centre to the GNSS antenna in the plane coordinate system is done during the manufacturing of the UAV, and cannot be repeated by the end user. In addition to the offset which assumes a horizontally positioned airplane, the attitude (yaw, pitch, roll) is needed for each point in time to accurately correct for the lever arm offset. To this end, a MEMS-based INS sensor is used. For this task, but also to relate the correct exposure time to GNSS time, synchronization of all critical events is indispensable. Absolute positions, obtained from combined GNSS and IMU observations, are delivered at 100 Hz. Without interpolation of the positions this frequency would already lead to an error of up to 20 cm, depending on the flight speed. An additional uncertainty emerges from the fact that end-user cameras very often just work according to a rolling shutter principle, i.e. an optimal triggering needs to take into account the time delay occurring here. A permanent link from the ground control unit needs to be available in order to provide the UAV with the RTK-GNSS information and enable a real-time computation of the position and attitude parameters.

The last major issue concerns the actual absolute positioning accuracy of each single position observation assigned to the individual camera shots. In an iterative procedure outliers are identified. In case of the Mavinci system this iterative bundle adjustment is implemented in the Photoscan software package (AGISOFT 2015). Initially all position parameters are included in the adjustment as observations with a pre-defined standard deviation of 2 cm in the horizontal plane and 3 cm in height. Detailed information on the workflow implemented in the software is not available. However, it can be assumed that after bundle adjustment the positional residuals are analysed and for all images showing large differences, the weight is decreased (i.e. the standard deviation increased) and the bundle adjustment is repeated. This process is iterated until the residuals of all remaining images with high weight are below a predefined threshold. In this way not only errors from the RTK solution (for instance caused by non-solved phase ambiguities) are taken into account, but in general also uncertainties originating from the entire calibration and correction process. In Fig. 1 an example image block is shown, indicating by colour for which image the provided position parameters are considered as being accurate (blue). Mostly the projection centre coordinates are introduced into the adjustment; IMU-based observations only play a minor role within the workflow because of lower quality. As automatically extracted points support tying images, this way in which GNSS-RTK measurements are included might be called partially integrated sensor orientation (JACOBSEN 2004).

As far as the source of reference information for the realization of the RTK-solution is concerned, the vendors advise to set up a temporary reference station close to or in the area of interest in order to achieve a high accuracy.
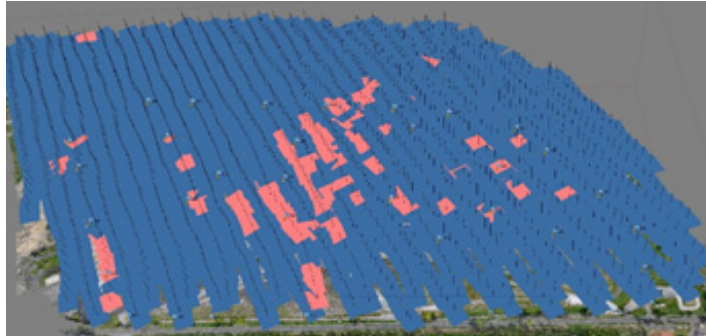
Fig. 1: Example block with images coloured according to the weights of the respective GNSS observations in the bundle adjustment: blue: estimated GNSS position accepted, position introduced with original weight; red: estimated absolute camera position with low weight in the bundle adjustment.

4 Datasets

Two UAV datasets were acquired in early 2014. While area 1 (stockpile) is characterized by large height variations and sandy/rocky terrain, in area 2 (Zollern) we find several buildings in a largely flat terrain. Both datasets reflect usual application areas for fixed-wing UAV projects.

Area 1 (stockpile): Data acquisition took place in April 2014. The area is close to the German city of Duisburg, covers 1100 x 600 m², and the height difference between the highest and the lowest point equals 50 m. The employed Mavinci Sirius Pro UAV, which is equipped with the mentioned 2-frequency GNSS receiver board, including RTK capabilities, was programmed to deliver a forward overlap of 85%, and a sidelap of 65% at 105 m average flight height. The Panasonic LumixGX1-Pancake14mm-PRO camera took in total 1900 images, at an average GSD of 2.7 cm. In addition to the North-South flight realized in the described pattern, a smaller block, covering 20% of the area, was captured in a West-East direction at 75 m average height, refer to Fig. 2. A temporary GNSS reference station was installed within the area.
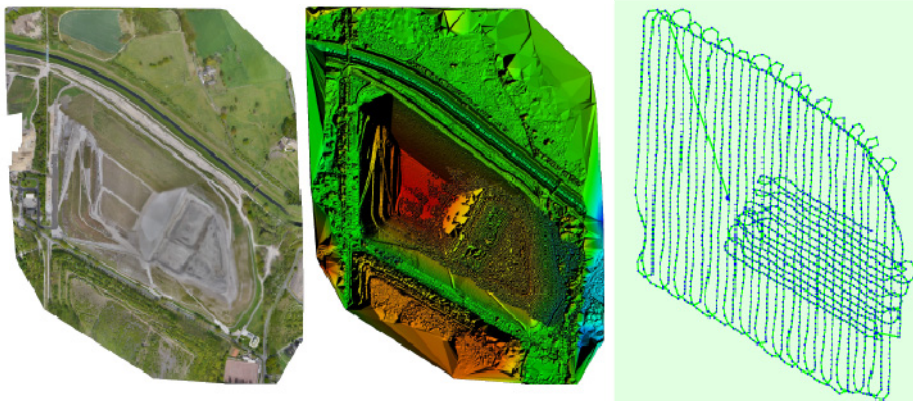

Fig. 2: Area 1, stockpile. Left: ortho image, middle: colour coded height model, right: flight plan.

Area 2 (Zollern): This dataset was acquired in the framework of the ISPRS scientific initiative *ISPRS Benchmark For Multi-Platform Photogrammetry* (NEX et al. 2015) in May 2014. The test site covers an area of 500 x 350 m², and contains mostly historic buildings of a former coal mine, which today are used as museums. Except

for two mine head towers no significant height variation is present. The flight parameters are similar to the ones used in area 1, refer to Fig. 3 for an overview. An important operational difference to area 1 is the access only to a regular Mavinci Sirius, without the GNSS-RTK option, hence this dataset was only used to analyse the impact of the cross flight pattern and GCP distribution. The camera used was of the same type as in area 1, but it was actually a different device.
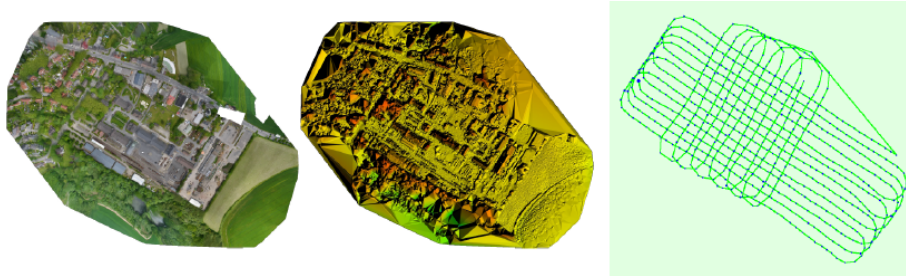

Fig. 3: Area 2, Zollern. Left: ortho image, middle: colour coded height model, right: flight plan.

Reference
For both areas well distributed 3D points were acquired. While in area 1 a standard RTK-GNSS system-based workflow was employed (35 points @ 3 cm standard deviation (3D)), in area 2 a static GNSS procedure was used to capture 34 points @ 2 cm standard deviation.

5 Experiments

Two different sets of experiment were carried out. The first one refers to the case where the UAV-based RTK-option is not used, but concentrates on the effect the cross-flight pattern has on the bundle block accuracy, and compares different GCP configurations. For this setup both datasets were employed. The second set of experiments additionally takes into account the RTK-option, while the remaining parameters are the same as in the first set. As the RTK-option was only available in area 1, this second part is only done with the stockpile dataset. Another important analysis concerns the impact that all different configurations have on self-calibration.

5.1 *Cross Flight and GCP Distribution*

The first set of experiments does not make use of the RTK-option provided by the UAV system, but assumes a traditional setup, where only ground control points are provided. The main objective of this first analysis concerns two questions: a) how does the number and distribution of GCP influence the accuracy, and b) does the flight pattern with cross layout and two different heights have an influence of the final bundle accuracy? To brighten those questions in both test areas four different configurations are tested: to use only four 3D points as GCPs and to use about half of measured points as GCPs (17 and 18 in areas 1 and 2, respectively), and in addition those two setups were evaluated with and without the additional images from the cross flight. To analyse the accuracy, the X Y Z residuals at the remaining check points, i.e. all measured 3D points which have not been used for the bundle block adjustment, are used. In all setups an individual self-calibration, including estimation of lens distortion parameters, was conducted.

In Fig. 4 RMSE values are shown, separated into horizontal RMSE, vertical RMSE and the combined 3D RMSE. While the left half shows results from area 1 (stockpile), the right half refers to area 2 (Zollern). The respective left columns refer to experiments where the additional images from the cross flights are used, while the right columns show results from the main flight only. All RMSE values, also for the next section, are summarized in Tab. 1. In area 1 the cross flight pattern does not have a significant impact on the overall accuracy. We only observe a typical error reduction when more GCPs are used: The 3D RMSE decreases from more than 20 cm to about 8 cm. Especially the errors in height are large when only 4 GCPs are used: while the XY RMSE

is below 5 cm, the RMSE in the Z component is about 20 cm, but it decreases down to 8 cm if 18 GCPs are used.

In area 2 the positive effect of the cross flight pattern onto the overall accuracy, but in particular onto the height accuracy, is obvious: already using only 4 GCPs in the cross pattern we obtain an overall 3D-RMSE of 3 cm, while it is almost 17 cm if only one flying height and -direction is used. The influence on the planimetric accuracy, however, is less significant. The reduction of the height error in the 4-GCP-case after using the additional images from the cross flight is large: the RMSE in Z is 16.5 cm without the use of the second image set and decreases to 2.4 cm when these images are used. In the next section we will elaborate on the question whether these large Z-errors are caused by block deformation. When more GCPs are used, however, the difference between the two configurations concerning the use of the cross flight disappear. In both sets we reach the limit of our evaluation procedure: given that the ground control measurements have a standard deviation of 2 cm, and the theoretical accuracy of points measured in the UAV image block is at the GSD-level ($\sigma = 2.5$ cm), the largest one-σ error according to the error propagation rule we are able to detect is approximately 3.2 cm. Therefore, although the small RMSE values support a clear trend towards GSD-level accuracy, the numbers are not statistically significant.
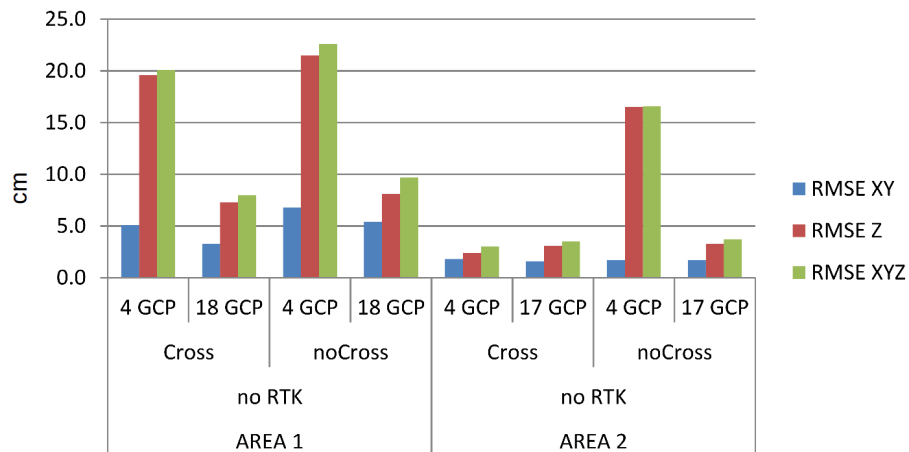

Fig. 4: RMSE of residuals at check points in area 1 and 2, with RTK disabled. Left columns with cross pattern used, right without. GCP: number of control points. In area 1, the number of check points is 31 if four and 17 if 18 GCPs are used. In area 2, the number of check points is 30 in case of four GCPs and 17 in case of 17 GCPs.

5.2 *UAV-based RTK, Cross Flight and GCP Distribution*

The second set of experiments has been conducted with the RTK-option enabled, i.e. the RTK-GNSS data attached to each image was integrated into the bundle adjustment according to section 3. As the airplane equipped with RTK-option was only available in area 1, the second area is omitted here. In addition to the configurations analysed in section 5.1, we also assess the result achieved without GCPs. From a practical point of view this variant is interesting, e.g. for disaster scenarios where GCPs might not be available, or any other near-real time application.
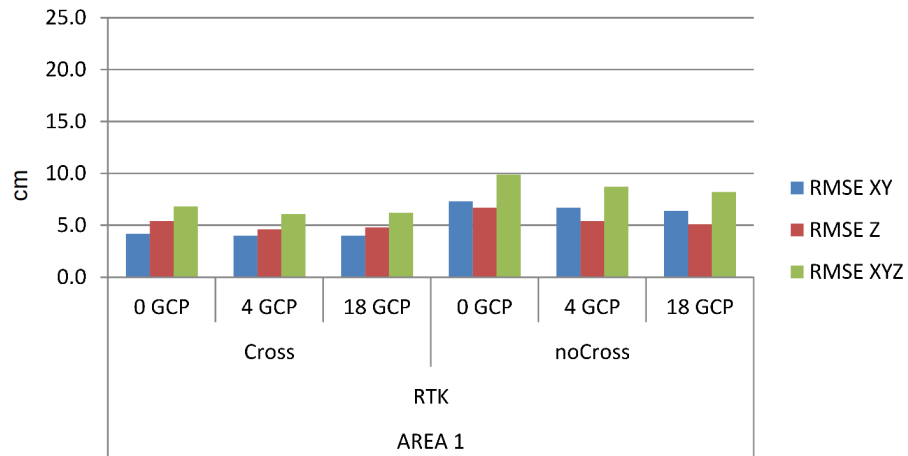
Fig. 5: RMSE of residuals at check points in area 1 with RTK enabled. Left column: cross-flight pattern used, right: no cross-flight pattern used. GCP: number of ground control points used. The number of check points is 35, 31, 17 if 0, 4 or 18 GCPs are used, respectively.

In Fig. 5 the respective RMSE charts for the RTK-supported bundle block adjustments are shown. First we observe that, similar to the experiments above, the relative change from the left to the right part, i.e. the influence of the cross-flight, is not really substantial, but visible, especially in the horizontal components which show smaller RMSE values for the cross configuration. More insight is available when different GCP configurations are compared. Even without any use of ground control the block accuracy is at an error range of 6.8 cm 3D RMSE when the cross flight pattern is used, and in XY the RMSE is below 5 cm. A closer look at the spatial distribution will help to understand the situation. In Fig 6, the XY residuals (green) are plotted in combination with height residuals (blue). The red scale bar in the left corner equals 10 cm. The arrangement of points is according to the given UTM-grid with cropped leading digits to leave the axis legend readable. The left plot in that figure is from the configuration: 4 GCPs, cross-flight, noRTK, while the right plot shows the same configuration, except for the fact that the RTK-option was enabled. On purpose we show the 4-GCP-configuration in order to be able to examine typical block deformation problems. The GCPs are distributed in the 4 corners of the block and in case no RTK is used (left plot in Fig. 6) the deformation, in particular towards the centre of the block is obvious. Closer to the GCPs those errors are reduced as expected. However, when we use the onboard RTK-option (right plot in Fig. 6), the deformation almost vanishes, and only in the southern part some Z-residuals increase to 8 cm.

Another important observation made in this second experiment show that the RMSE does not improve much with an increasing number of GCPs. For most configurations it is nearly constant. Here, once more we look at the error propagation. While for the UAV image block we assume a point measurement accuracy again of $\sigma = 2.5$ cm, the GCPs acquisition in area 1 was a bit more inaccurate compared to area 2, and we assume $\sigma = 3$ cm. These numbers lead to a combined standard deviation of approximately $\sigma = 4$ cm of the differences. Although we see a trend in the RMSE values towards a better accuracy when more GCPs are introduced, we cannot evaluate the quality more reliably.
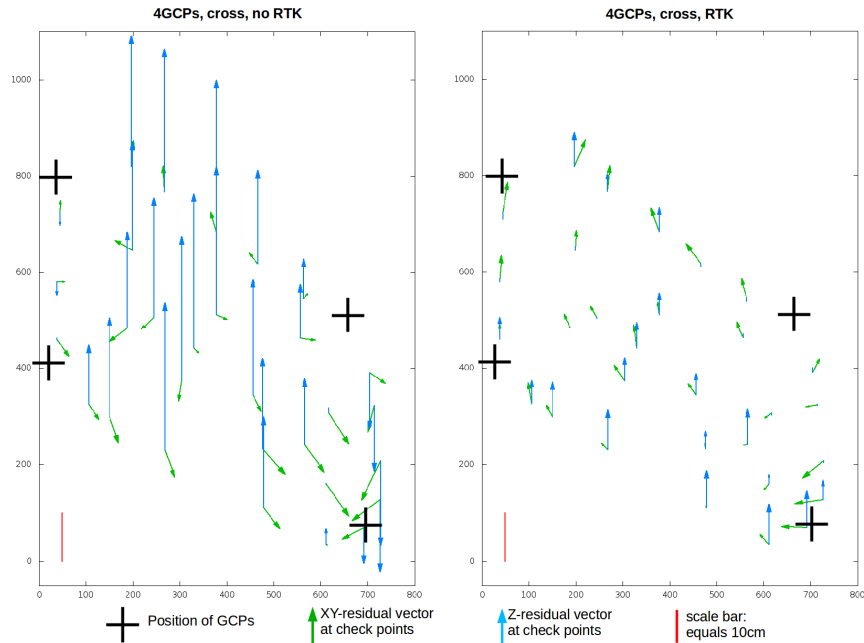
Fig. 6: Spatial plot of residuals, separated by XY- and Z-component. In both cases: use of 4 GCPs (black crosses), cross flight configuration, left: RTK-option disabled, right: RTK enabled.

Tab. 1 summarizes the results for all configurations: the left columns show the non-RTK solutions from the last section, while the right hand side shows the results from this section with enabled RTK.

Tab. 1: Horizontal / Z (3D) RMSE (cm) for all configurations as shown in Figs. 4, 5, and 6.

	No RTK (see Fig. 4)		RTK enabled (see Fig. 5)	
	Cross	**No Cross**	**Cross**	**No Cross**
Area 1, no GCPs	-----	----	4.2/5.4 (6.8)	7.3/6.7 (9.9)
Area 1, 4 GCPs	5.1/19.6 (20.1) (*Fig. 6, left*)	6.8/21.5 (22.6)	4.0/4.6 (6.1) (*Fig. 6, right*)	6.7/5.4 (8.7)
Area 1, 18 GCPs	3.3/7.3 (8.0)	5.4/8.1 (9.7)	4.0/4.8 (6.2)	6.4/5.1 (8.2)
Area 2, 4 GCPs	1.8/2.4 (3.0)	1.7/16.5 (16.6)	----	----
Area 2, 17 GCPs	1.6/3.1 (3.5)	1.7/3.3 (3.7)	----	----

5.3 *Impact on Self-Calibration*

In this section we further analyse the parameters of the interior orientation, i.e. focal length and principal point offset. Radial and tangential distortion parameters are estimated as well. In our experiments, however, they do not differ significantly for the different setups. In the projective camera model used in the employed software a

scale factor for the pixel aspect is estimated as well, hence there are actually 4 parameters: px and py for the principal point offset with respect to image centre, and cx and cy which are actually composed as cx = mx*f, and cy = my*f, while mx and my are scale factors in column and row direction, respectively, and f the focal length. In Fig. 7 the values for px, py, cx, and cy are plotted for all experiments. The values cx and cy are differences to the approximations derived from EXIF headers. The upper diagram is for area 1, while the lower one refers to area 2.
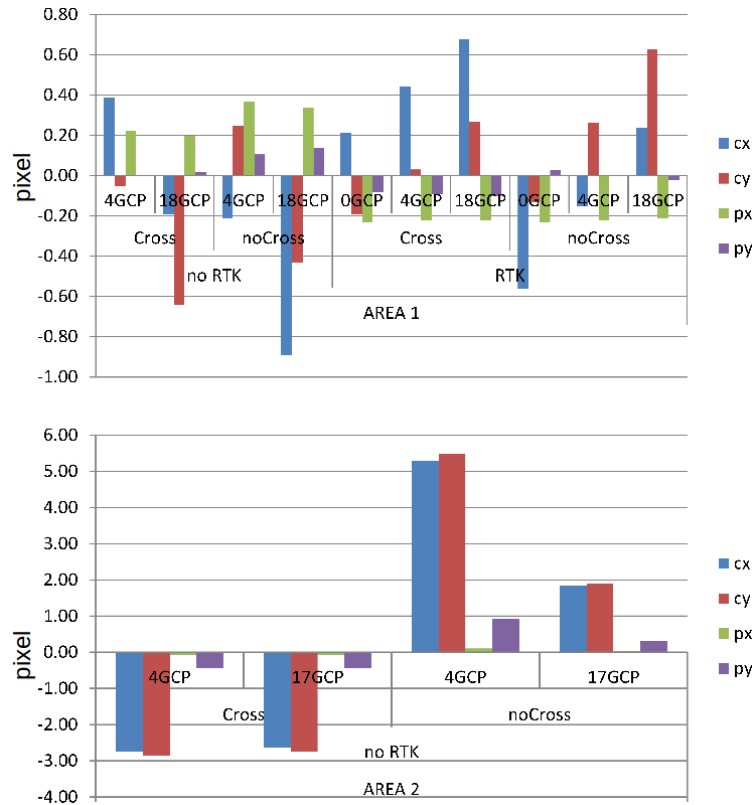

Fig. 7: Principal point offset (px, py) and focal length difference to initial values (cx,cy) for all experiments. Values in pixel. Note the different scaling in y.

While the principal point offset does only vary in a random pattern and with non-significant size, we can observe a certain trend for the focal length. The variations are small; they are 10 pixels at maximum for area 2, which is equivalent to 35 μm. However, given the fact that in areas 1 and 2 the same type of camera was used, the variation in cx and cy is about ten times larger in area 2, compared to area 1. From this we might conclude that the actual estimation of the focal length is more uncertain in the flat area of Zeche Zollern (area 2), while in area 1 the flight configuration and surface variation helps to estimate a more stable set of parameters. Unfortunately, a deeper analysis of the statistical significance of differences observed in Fig. 7 or of correlations between was not possible, because Agisoft does not deliver precision values for the unknowns.

5.4 *Synchronization of Sensor Observations: Remaining Errors*

A very interesting observation can be made when estimated sensor locations from the GNSS-RTK approach are compared to the finally derived positions after GCP-supported bundle adjustment. The upper part of Fig. 8

shows a diagram which indicates the airplane speed during the operation, and in the lower part distances between GNSS-RTK-based and finally adjusted sensor positions are plotted. During the flight in area 1 it was quite windy and this is also reflected in the speed chart: UAV velocities vary from about 50 km/h to 95 km/h. The lower diagram indicates some significant differences. The sign of the differences (offsets) alternates per strip, and the amplitude varies from 10 cm to 20 cm. The charts in Fig. 8 allow to argue that there is a certain correlation between the speed of the airplane and the observed offsets. Unfortunately, a rigorous analysis, e.g. by linear regression, is not possible because from the flight log the accurate time of image exposure cannot be retrieved. A possible explanation for the offsets can be a certain time gap between the position observation and the camera triggering. In order to roughly estimate the time gap a simple computation has been carried out: at a speed of about 55 km/h (15 m/sec) an average offset of 10 cm was registered, this means a delay of about 6 ms, while for the higher speed of 85 km/h (24 m/s) an average difference of 20 cm is visible, leading to a time gap of 8 ms. It must be noted that without more detailed sensor readings, e.g. also from the IMU and at sufficient frequency, a statistically sound analysis is not possible.

The absolute errors of 10 cm to 20 cm do not occur in the check point residuals, even if no GCPs are used (refer to Tab. 1 and Fig. 5). The 2D RMSE is about 4 cm. The explanation for this is the flight in regular strips and the change of heading of the airplane at the end of every strip. Thus, the absolute error averages out. Actually, the mean offset (see blue dotted line in lower chart of Fig. 8) is 1.5 cm.
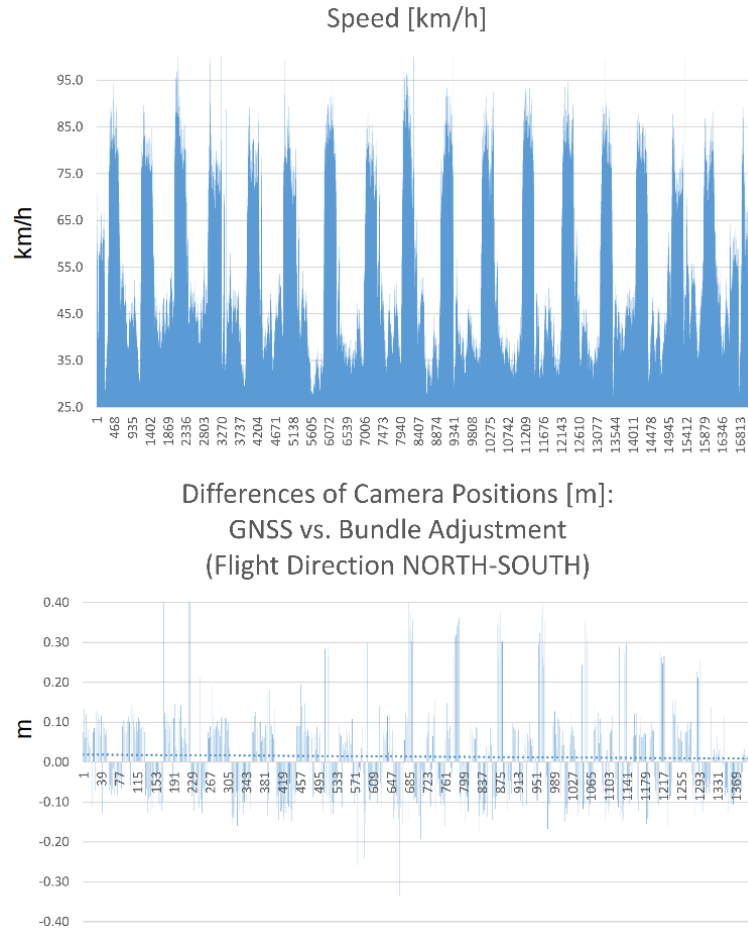
Fig. 8: Airplane speed as a function of time and difference in projection centre positions: GNSS-RTK solution vs. bundle adjustment using GCPs. Blue dotted line: average at 1.5 cm.

6 Discussion, Conclusions and Outlook

Concerning the first objective of this research, which was to analyse the influence of a cross-flight pattern and the GCP distribution on the bundle block adjustment we saw a quite different behaviour in the two test areas. In area 1 the residuals at checkpoints, in case the images from the cross-flight were used, were of a similar size as in the case where only the images from the main flight were utilized. The main reason for this is probably that area 1 shows some natural height elevation changes, leading to fewer problems in self-calibration. This assumption is confirmed by the analysis of the internal orientation parameters: the variation of the focal length is negligible. However, the XY error is always a bit smaller when the second image set is used. Thus, we might conclude that the different flight directions contribute to a more accurate estimation of the principal point. Probably due to a lack of natural elevation differences in area 2, the positive effect the cross-flight pattern has onto the final accuracy is significant, first of all in the Z component. The relatively large variation of the calibrated focal length supports the assumption of an inaccurate self-calibration. When many GCPs are introduced into the bundle adjustment, the difference in RMSE between those two setups is not visible anymore: obviously the camera self-calibration improves or remaining errors are better compensated through the exterior orientation,

respectively, when more GCPs are provided. Although the applied software does not provide statistic measures on the adjusted unknowns it is likely that the parameters of external and internal orientation are highly correlated. Thus, it is difficult to use self-calibration if the terrain is not undulated or cross-flight patterns at different altitudes are not possible. This might also influence the final accuracy. In those cases a well pre-calibrated (metric) camera should be used (LUHMANN et al. 2015).

As far as the second aim of this paper is concerned, namely to quantify whether the influence of the integrated RTK-UAV workflow provides an enhancement on absolute image orientation accuracy, we can discuss some findings here as well. Because of the effects in conjunction with possibly less accurate 3D point measurements we cannot conclude on the absolute accuracy obtainable, however, we can make very important observations when we compare the different setups. Even if no GCPs are introduced, the accuracy in object space is better compared to the setup without the use of the RTK-UAV option, but with more GCPs enabled (the 3D RMSE is 1 cm smaller). From this, we can draw the conclusion that the absolute block orientation accuracy can be enhanced significantly by using the onboard RTK solution. Block deformation is a typical problem in UAV image blocks, especially when the block is not supported by well distributed GCPs. This observation was also made here, refer to Fig. 6, but the problem is mitigated considerably when using support through the RTK-option, at least in our experiments the block deformation was hardly visible in that case. Despite the competitive results obtained from the GNSS-RTK-supported solution we observed synchronization errors resulting in absolute positional offsets. In the regular image block these errors were obviously averaged out, but in less regular blocks or free flights those errors need to be considered.

From all these finding we can derive some important hints for the practice. First of all, if the terrain does not show much undulation we would advise to plan a cross-flight, at least in some parts. The inclusion of RTK-based image position observations into the UAV processing workflow turned out to have a very positive effect, in particular onto the height component. With our experiments we showed that even a UAV-RTK-only solution delivers results which are superior to the traditional completely indirect sensor orientation. In those cases, however, it is important to provide at least some check points with very high accuracy, e.g. as delivered through static GNSS, in order to be able to thoroughly validate the obtained results. This is especially important in the light of the detected remaining synchronization uncertainties.

In the future, we expect to see more RTK-supported UAV image processing hardware and processing pipelines. Typical applications fields like multi-temporal data acquisition (vegetation monitoring, building construction monitoring) would definitely benefit from the demonstrated accuracies that we obtained without the inclusion of ground control and that might be sufficient. UAV-based damage mapping is another field of interest (VETRIVEL et al. 2015). In some areas like forests GCP acquisition might not be possible, and if data from previous epochs or old maps are to be combined with new images, accurate georeferencing is indispensable. One of the next steps would also include the integration of such a RTK-GNSS device plus INS like the Trimble BD 935 in a rotary wing platform, potentially directly mounted at the gimbal, or even at the camera (TRIMBLE INC. 2015). If it were possible to also approximate the attitude of the optical axis, in addition to a precise position, we could expect at least a faster and more efficient camera orientation. ALSADIK et al. (2013) already showed that the knowledge of approximate camera locations and viewing direction could decrease processing time tremendously and at the same time increase the overall reliability.

Acknowledgements

References

AGISOFT, 2015: Agisoft Photoscan software. – http://www.agisoft.com (11.11.2015).

ALSADIK, B., GERKE, M. & VOSSELMAN, G., 2013: Automated camera network design for 3D modeling of cultural heritage objects. – Journal of Cultural Heritage **14**(6): 515–526. http://doi.org/10.1016/j.culher.2012.11.007.

BÄUMKER, M., PRZYBILLA, H.-J. & ZURHORST, A., 2013: Enhancements in UAV Flight Control and Sensor Orientation. – The International Archives of the Photogrammetry, Remote Sensing and Spatial Information Sciences **XL–1/W2**: 33–38. http://doi.org/10.5194/isprsarchives-XL-1-W2-33-2013.

CRAMER, M., 2001: Genauigkeitsuntersuchungen zur GPS/INS-Integration in der Aerophotogrammetrie. PhD Dissertation, Deutsche Geodätische Kommission, Reihe C, 537, 120p.

COLOMINA, I. & MOLINA, P., 2014: Unmanned aerial systems for photogrammetry and remote sensing: A review. – ISPRS Journal of Photogrammetry and Remote Sensing, **92**(0): 79–97. http://doi.org/10.1016/j.isprsjprs. 2014.02.013.

ELING, C., KLINGBEIL, L., WIELAND, M. & KUHLMANN, H., 2014: Direct georeferencing of micro aerial vehicles – system design, system calibration and first evaluation tests. – PFG – Photogrammetrie, Fernerkundung, Geoinformation **4**: 227–237.

FÖRSTNER, W. & STEFFEN, R., 2007: Online Geocoding and Evaluation of Large Scale Imagery without GPS. – Photogrammetric Week 2007: 243–253, Herbert Wichmann.

JACOBSEN, K., 2004: Direct Integrated Sensor Orientation – Pros and Cons. – The International Archives of the Photogrammetry, Remote Sensing and Spatial Information Sciences XXXV/W3: 829–835.

LUHMANN, T., FRASER, C. & MAAS, H.-G., 2015: Sensor modelling and camera calibration for close-range photogrammetry – ISPRS Journal of Photogrammetry and Remote Sensing, in press, 10 p. http://dx.doi.org/10.1016/j.isprsjprs.2015.10.006.

MAVINCI, 2015: SIRIUS PRO Surveying UAS. – http://www.mavinci.de/en/siriuspro (11.8.2015).

NEX, F., GERKE, M., REMONDINO, F., PRZYBILLA, H.-J., BÄUMKER, M. & ZURHORST, A., 2015: ISPRS benchmark for multi - platform photogrammetry. – ISPRS Annals of the Photogrammetry, Remote Sensing and Spatial Information Science **II–3/W4**: 135–142. http://doi.org/10.5194/isprsannals-II-3-W4-135-2015.

NEX, F. & REMONDINO, F., 2014: UAV for 3D mapping applications: a review. – Applied Geomatics **6**(1): 1–15. http://doi.org/10.1007/s12518-013-0120-x.

NOCERINO, E., MENNA, F., REMONDINO, F. & SALERI, R., 2013: Accuracy and Bock Deformation Analysis in Automatic UAV and Terrestrial Photogrammetry – Lessons learnt. – ISPRS Annals of the Photogrammetry, Remote Sensing and Spatial Information Science **II-5/W1**: 203–208. http://doi.org/10.5194/isprsannals-II-5-W1-203-2013.

PFEIFER, N., GLIRA, P. & BRIESE, C., 2012: Direct Georeferencing With on Board Navigation Components of Light Weight UAV Platforms. – The International Archives of the Photogrammetry, Remote Sensing and Spatial Information Sciences XXXIX/W7: 487–492.

PRZYBILLA, H.-J., REUBER, C., BÄUMKER, M. & GERKE, M., 2015: Untersuchungen zur Genauigkeitssteigerung von UAV-Bildflügen. – 35. Wissenschaftlich-Technische Jahrestagung der DGPF **24**: 45–54.

REHAK, M., MABILLARD, R. & J. SKALOUD, J., 2014: A micro aerial vehicle with precise position and attitude sensors. – PFG – Photogrammetrie, Fernerkundung, Geoinformation **4**: 239–251.

RUMPLER, M., DAFTRY, S., TSCHARF, A., PRETTENTHALER, R., HOPPE, C., MAYER, G. & BISCHOF, H., 2014: Automated End-to-End Workflow for Precise and Geo-accurate Reconstructions using Fiducial Markers. – ISPRS Annals of the Photogrammetry, Remote Sensing and Spatial Information Science **II–3**: 135–142. http://doi.org/10.5194/isprsannals-II-3-135-2014.

SCHNEIDER, J., LÄBE, T. & FÖRSTNER, W., 2014: Real-Time Bundle Adjustment with an Omnidirectional Multi-Camera System and GPS. – 4th International Conference on Machine Control & Guidance: 98–103.

SENSEFLY SA, 2015: eBee RTK. – https://www.sensefly.com/drones/ebee-rtk.html (11.8.2015).

TRIMBLE INC., 2015: Trimble bd935-ins. – http://intech.trimble.com/oem_gnss/receiver_boards/trimble_bd935-ins (11.8.2015).

VETRIVEL, A., GERKE, M., KERLE, N. & VOSSELMAN, G., 2015: Identification of damage in buildings based on gaps in 3D point clouds from very high resolution oblique airborne images. – ISPRS Journal of Photogrammetry and Remote Sensing **105**: 61–78.

WATTS, A.C., AMBROSIA, V.G. & HINKLEY, E.A., 2012: Unmanned Aircraft Systems in Remote Sensing and Scientific Research: Classification and Considerations of Use. – Remote Sensing **4**(12): 1671–1692. http://doi.org/10.3390/rs4061671.

YANG, B. & CHEN, C., 2015: Automatic registration of UAV-borne sequent images and LiDAR data. – ISPRS Journal of Photogrammetry and Remote Sensing **101**: 262–274. http://doi.org/10.1016/j.isprsjprs.2014.12.025.

Addresses of the authors:

Dr.-Ing. MARKUS GERKE, University of Twente, Faculty of Geo-Information Science and Earth Observation – ITC, Department of Earth Observation Science, Hengelosestraat 99, Enschede, The Netherlands. Tel.: +31-53-4874-522, e-mail: m.gerke@utwente.nl

Prof. Dr.-Ing. HEINZ-JÜRGEN PRZYBILLA, Bochum University of Applied Sciences, Department of Geodesy, Lennershofstr. 140, 44801 Bochum, Germany. Tel.: +49-234-32-10517, e-mail: heinz-juergen.przybilla@hs-bochum.de